Journal of Power Sources 217 (2012) 400–406

Contents lists available at SciVerse ScienceDirect

Journal of Power Sources

journal homepage: www.elsevier.com/locate/jpowsour

Synthesis of pure phase disordered $LiMn_{1.45}Cr_{0.1}Ni_{0.45}O_4$ by a post-annealing method

D. Liu [a], J. Hamel-Paquet [a], J. Trottier [a], F. Barray [a], V. Gariépy [a], P. Hovington [a], A. Guerfi [a], A. Mauger [b], C.M. Julien [c], J.B. Goodenough [d], K. Zaghib [a,*]

[a] Energy Storage and Conversion, Research Institute of Hydro-Québec, Varennes, Québec, Canada J3X 1S1
[b] Université Pierre et Marie Curie – Paris 6, Institut de Minéralogie et Physique de la Matière Condensée (IMPMC), 4 place Jussieu, 75005 Paris, France
[c] Université Pierre et Marie Curie – Paris 6, Physicochimie des Electrolytes, Colloïdes et Sciences Analytiques (PECSA), UMR 7195, 4 place Jussieu, 75005 Paris, France
[d] The University of Texas at Austin, Austin, TX 78712, USA

HIGHLIGHTS

- High purity $LiMn_{1.45}Cr_{0.1}Ni_{0.45}O_4$ has been obtained.
- The B-site of the spinel is partially ordered at the scale of the nearest neighbors, fully disordered at the scale of the nanometer.
- The electrochemical properties are improved with respect to a commercial sample.

ARTICLE INFO

Article history:
Received 16 May 2012
Received in revised form
14 June 2012
Accepted 16 June 2012
Available online 23 June 2012

Keywords:
Li-ion
5V system
Cathode
$LiMn_{1.45}Cr_{0.1}Ni_{0.45}O_4$
Post-annealing

ABSTRACT

A post-annealing strategy at 600 °C was used to modify the oxygen deficiency during synthesis of a spinel $LiMn_{1.45}Cr_{0.1}Ni_{0.45}O_4$ cathode for lithium-ion batteries. Structural analyses revealed that post-annealing is an effective way to eliminate the impurity phase without changing the $Fd\bar{3}m$ space group. The substitution of a small amount of Cr leads to better rate performance along with cyclability at room temperature, compared to the commercial $LiMn_{1.5}Ni_{0.5}O_4$. $LiMn_{1.45}Cr_{0.1}Ni_{0.45}O_4$ delivered a reversible capacity of ~115, 104, 95 and 40 mAh g^{-1} at 0.2C, 1C, 2C and 5C, respectively. While commercial $LiMn_{1.5}Ni_{0.5}O_4$ offered a lower reversible capacity of ~110, 98, 85 and 20 mAh g^{-1} at the same C rates. After 125 cycles, about 99% of reversible capacity was retained for the $LiMn_{1.45}Cr_{0.1}Ni_{0.45}O_4$, while about 6% of capacity loss was obtained after 125 cycles for the commercial $LiMn_{1.5}Ni_{0.5}O_4$. Electrochemical impedance spectroscopy measurements revealed that the $LiMn_{1.45}Cr_{0.1}Ni_{0.45}O_4$ had a smaller surface resistance, which may be due to the segregation of Ni from the surface to the bulk.

© 2012 Elsevier B.V. All rights reserved.

1. Introduction

Developing cathode materials with high energy densities is one of the key challenges for adopting the lithium-ion battery technology for hybrid electric vehicle (HEV) and plug-in hybrid electric vehicle (PHEV) applications. A high energy density can be obtained either by high voltage or high capacity [1,2]. With a high operating voltage around 4.7 V and a practical capacity (about 130 mAh g^{-1}) comparable to that of $LiCoO_2$ (~140 mAh g^{-1}) and $LiFePO_4$ (~160 mAh g^{-1}), spinel $LiMn_{1.5}Ni_{0.5}O_4$ provides a higher specific energy (~610 Wh kg^{-1}) than many commercialized compounds.

Previous studies in the literature have reported that there are two types of $LiMn_{1.5}Ni_{0.5}O_4$ (denoted LMN) depending on the ordering of Ni/Mn in the octahedral sites, a disordered LMN and an ordered LMN [3–6]. In the disordered spinel, where transition-metal ions are randomly distributed at octahedral 16*d* sites, the $Fd\bar{3}m$ space group is observed. The Li at a tetrahedral 8*a* site moves via a vacant octahedral 16*c* site in an 8*a*-16*c* diffusion path. In contrast, the ordered LMN has a $P4_332$ space group with Li atoms located at 8*c* sites; the octahedral vacant 16*c* sites are split into ordered 4*a* and 12*d* sites with a ratio of 1:3 to form diffusion paths 8*c*-4*a* and 8*c*-12*d* (Fig. 1). Ordering of the Ni(II) and Mn(IV) retards the lithium diffusivity [7] and therefore lowers the rate capability [3,8,9].

However, the synthesis of disordered LMN is often accompanied by oxygen loss at high temperature (>715 °C), which results in nonstoichiometric $LiMn_{1.5}Ni_{0.5}O_{4-\delta}$ [3]. Oxygen deficiency in LMN

* Corresponding author. Tel.: +1 450 652 8019; fax: +1 450 652 8424.
E-mail address: zaghib.karim@ireq.ca (K. Zaghib).

0378-7753/$ – see front matter © 2012 Elsevier B.V. All rights reserved.
http://dx.doi.org/10.1016/j.jpowsour.2012.06.063

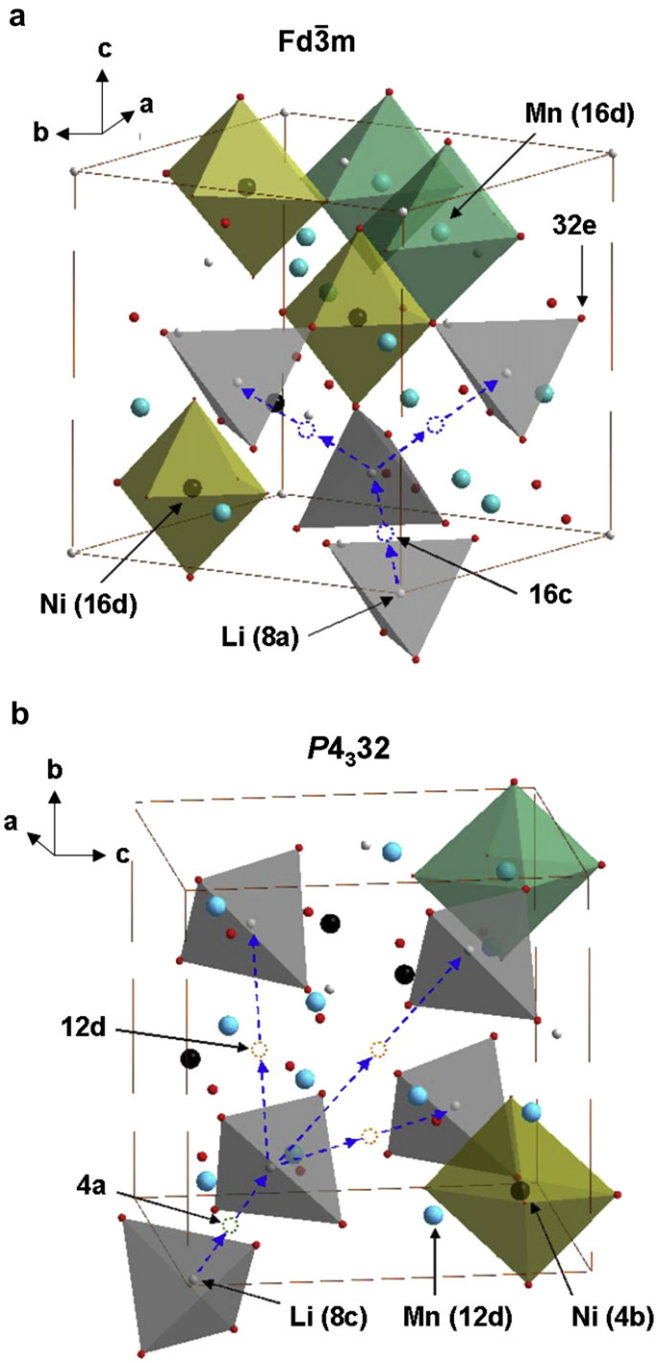

Fig. 1. Lithium diffusion path in $LiMn_{1.5}Ni_{0.5}O_4$ spinel with space group of (a) $Fd\bar{3}m$ and (b) $P4_332$.

introduces a $Li_xNi_{1-x}O$ impurity and partially reduces Mn^{4+} to Mn^{3+} to satisfy local charge neutrality; the Mn^{4+}/Mn^{3+} couple exhibits a step in the $V(x)$ profile at ~4.1 V *vs.* Li. To suppress the $Li_xNi_{1-x}O$ impurity phase and improve the electrochemical performance, various cation substitutions have been pursued [10–13]. Recently, we found that equal amounts of Cr^{3+} substitution for Ni^{2+} and Mn^{4+} improves the rate capability especially for $LiMn_{1.45}Cr_{0.1}Ni_{0.45}O_4$, due to the segregation of Ni from the surface to the bulk as indicated by energy-dispersive x-ray (EDX) analyses [12]. However, there are still some Ni-based impurities and a small 4.1 V Mn^{3+}/Mn^{4+} redox plateau for the whole series of Cr-substituted LMN. In this work, we used a post-annealing strategy at lower temperature to modify the oxygen deficiency and suppress the Mn^{3+} content while maintaining the disordered structure. With the post-annealing strategy, a pure $LiMn_{1.45}Cr_{0.1}Ni_{0.45}O_4$ disordered phase was successfully synthesized. The structural analyses and electrochemical properties between our final sample and a commercial one, from Energy Innovation Group (EIG), Korea, were also compared in this study.

2. Experimental

2.1. Synthetic procedure

Spinel $LiMn_{1.45}Cr_{0.1}Ni_{0.45}O_4$ samples were prepared by a post-annealing method under the assistance of oxalic acid as previously described [12,14]. The procedure involves the precipitation of stoichiometric amounts of manganese, lithium, nickel acetates (99% Aldrich) and chromium nitrate (99% Aldrich) precursors by adding oxalic acid solution, followed by pre-firing the precursors at 500 °C for 6 h and then another 12 h at 800 °C. After grinding, the black powders were post-annealed for 48 h at 600 °C to get the final sample. All heating treatment processes were carried out in air.

2.2. Structural and physical characterization

Powder x-ray diffraction (XRD) patterns were step-scan recorded on a Philips x-ray diffractometer equipped with Cu Kα radiation in steps of 0.02° with a step time of 10 s over the range $10° < 2\theta < 90°$ for each sample. The XRD results were refined with the FULLPROF program. Scanning electron microscopy (SEM) images of the final samples were obtained with an electronic microscope Hitachi model HD-2700 with 200 kV, 5 kV and 3 kV operating potential. Fourier transform infrared (FTIR) spectra were recorded with a Fourier transform interferometer (model Bruker IFS 113v) with KBr pellets. The characteristic vibrational bands of the metal-oxygen bonds between 400 and 700 cm^{-1} were used to examine the ordering of cations in the 16*d* sites of the spinel lattice. The magnetic measurements were performed in an SQUID magnetometer (Quantum Design MPMS-5S).

2.3. Electrochemical studies

The electrochemical performance of each sample was evaluated with a standard CR2032 coin cell composed of a cathode, lithium anode, a Celgard polypropylene separator, and $LiPF_6$ in 1:1 ethylene carbonate/diethylene carbonate (EC/DEC) as electrolyte. The cathode electrode contains about 89 wt.% active material, 6 wt.% conductive carbon, and 5 wt.% PVdF binder. All cells were fabricated in an argon-filled glove box and galvanostatically cycled with a VMP-cycler (Biologic, France) at 25 °C between 3.5 and 4.9 V.

3. Results and discussion

Fig. 2 presents the XRD patterns of the spinel samples calcined at different temperatures. The impurity phase at ca. $2\theta = 37.7$ and 43.6° can be seen to increase with increasing temperature from 700 to 900 °C as a result of the oxygen loss at high temperature. This can be attributed to the presence of rock salt impurity often met in such compounds. The amount of impurity increases with the synthesis temperature T_s. This increase is correlated with an increase of the lattice parameter by 0.15% between $T_s = 700$ and 900 °C, proof that some oxygen is removed from the host. It is not possible to identify the nature of the impurity, although it is presumably associated to Li_2MnO_3, because its composition varies with T_s, as can be seen in Fig. 2 from the shit of the impurity peak with T_s. Interestingly, the impurity diffraction lines are absent in our $LiMn_{1.45}Cr_{0.1}Ni_{0.45}O_4$

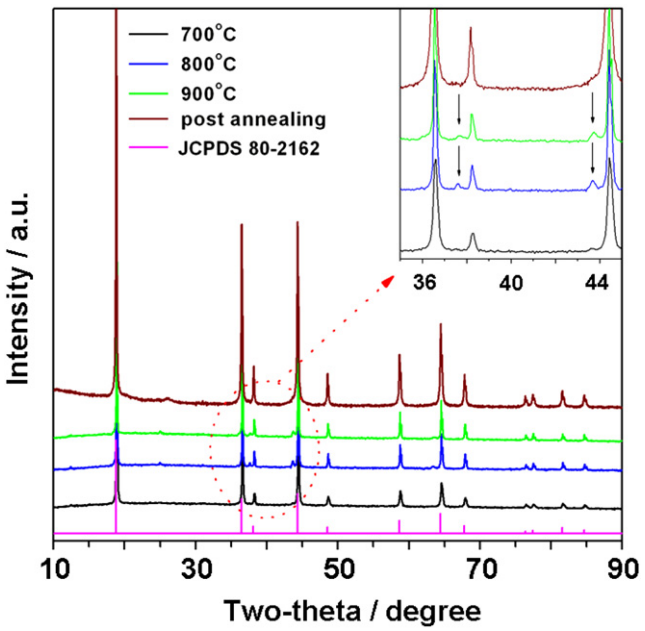

Fig. 2. XRD patterns of the spinel samples at different steps of the synthesis: at different temperatures up to 900 °C before annealing, and for the final sample, post-annealed at 600 °C for 48 h. Inset shows the magnified peaks between $2\theta = 35–45°$.

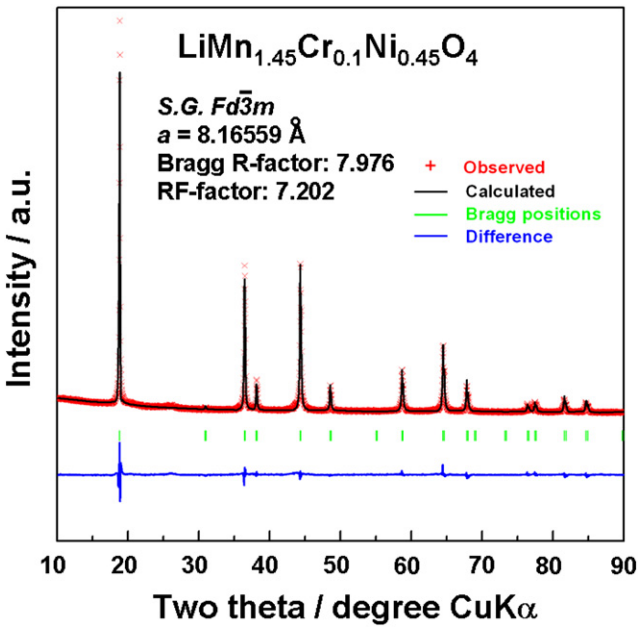

Fig. 3. Rietveld refinement profiles of the XRD data for the final $LiMn_{1.45}Cr_{0.1}Ni_{0.45}O_4$ sample.

sample after it was re-annealed at 600 °C, indicating that post annealing is an effective way to eliminate the impurity phase. Moreover, the lattice parameter is increased by 0.34% in the annealing process, so that oxygen is reinserted. On the other hand, it has been reported that the spinel LMN undergoes a thermally induced order/disorder transition at ~700 °C [5]. Therefore, we assume that re-annealing at 600 °C only helps to modify the oxygen deficiency while maintaining the disordered structure. Meanwhile, substitution of Cr^{3+} for Ni^{2+} and Mn^{4+} not only helps to keep the Mn^{4+} oxidation state unchanged ($2Cr^{3+} = Ni^{2+} + Mn^{4+}$), but also introduces greater disorder of the B-site cations in LMN [12]. In order to verify the order/disorder of our final $LiMn_{1.45}Cr_{0.1}Ni_{0.45}O_4$ sample, Rietveld refinement of XRD data was carried out with the Fullprof program in the $Fd\bar{3}m$ space group with Li in 8*a* sites and transition metals statistically distributed in 16*d* sites. The well-fitted refinement profile given in Fig. 3 for the final sample confirms that the $LiMn_{1.45}Cr_{0.1}Ni_{0.45}O_4$ spinel still retains the disordered structure (space group $Fd\bar{3}m$). Moreover, Rietveld refinement also gives the cubic lattice parameter a=8.16,559 Å, which is close to the value for ordered LMN [3,15], but different from our previous result of 8.17,846 Å [12]. Since the ionic radius of Mn^{4+} is smaller than that of Mn^{3+} and the increased lattice parameter with the presence of Mn^{3+} results from the oxygen deficiency at high temperature, it is reasonable to conclude that there are fewer Mn^{3+} ions after re-annealing at 600 °C. From the Scherrer's formula

$$L = 0.9\lambda/B\cos\theta \quad (1)$$

where λ is the X-ray wavelength and B is the width at an intensity equal to half maximum (FWHM), the coherent length, L, is estimated from the XRD pattern to be $L = 67$ nm.

FTIR spectroscopy, another technique to distinguish the order from disorder in LMN [5,6,9], was also performed in this work to further investigate the order/disorder change of our samples after different procedures. The FTIR spectra are compared in Fig. 4. The characteristic bands [5,9] (at around 430, 468, 558, and 650 cm^{-1}) corresponding to the cation-ordered structure only appear in the spectra of the sample calcined at 700 °C and are absent in the spectra of the other samples, which confirms that the order/disorder transition only occurs at ~700 °C [3,5,8]. In addition, a very low intensity ratio of the two bands at 588 and 619 cm^{-1} in the final sample (post-annealed at 600 °C) in Fig. 4 indicates that the final $LiMn_{1.45}Cr_{0.1}Ni_{0.45}O_4$ sample mostly consists of cation-disordered ($Fd\bar{3}m$) phase with a very small amount of ordered ($P4_332$) phase [5,9]. Fig. 5 shows the FTIR spectra of our final $LiMn_{1.45}Cr_{0.1}Ni_{0.45}O_4$ sample and a commercial LMN for comparison. In contrast, the high intensity ratio of the two bands at 588 and 619 cm^{-1} in the spectra of the commercial sample reveals that it has more ordered phase in the spinel structure. Despite the so-called "cation-disordered phase" that corresponds to the $Fd\bar{3}m$ space group or O_h^7 spectroscopic symmetry, we notice the FTIR

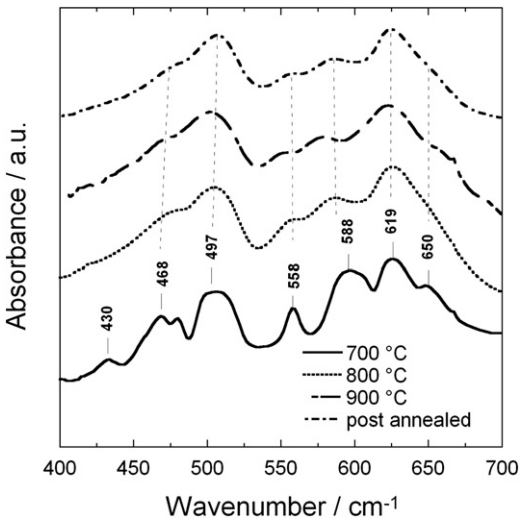

Fig. 4. Infrared spectra of the $LiMn_{1.45}Cr_{0.1}Ni_{0.45}O_4$ samples obtained at different steps of the synthesis: at different temperatures up to 900 °C before annealing and for the final sample, post-annealed at 600 °C for 48 h.

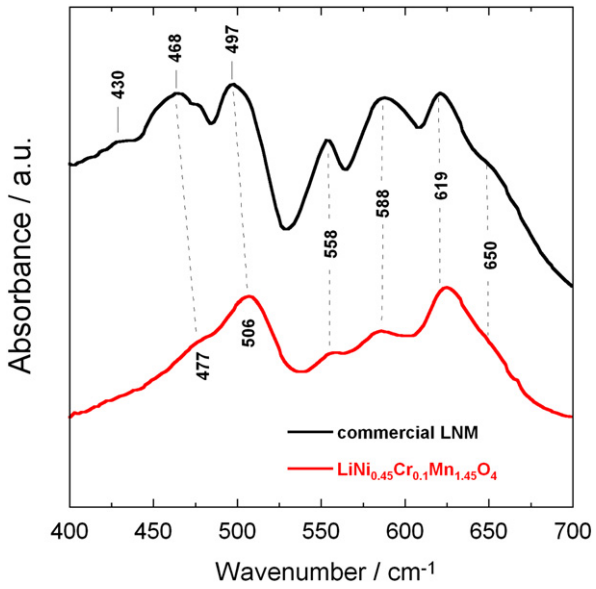

Fig. 5. Infrared spectra of our final $LiMn_{1.45}Cr_{0.1}Ni_{0.45}O_4$ sample and a commercial sample.

spectrum has well-resolved stretching modes in contrast to the typical spinel $LiMn_2O_4$ exhibiting overlapping broad bands. These vibrational-spectroscopy results can be understood in terms of short-range Ni^{2+}, Mn^{4+} cation ordering on the octahedral sites.

The variation with thermal treatment of the particle size and morphology were examined by SEM. Images of the disordered $LiMn_{1.45}Cr_{0.1}Ni_{0.45}O_4$ displayed in Fig. 6 represent the well-crystallized material with a particle size in the range of 0.5–2 μm. The micrograph (Fig. 6b) reveals that the post-annealing at 600 °C promotes well-faced grains of regular shape characteristic of the cubic spinel morphology. These results are consistent with the data obtained from XRD measurements.

The magnetization $M(H)$ curves of our final 600 °C post-annealed $LiMn_{1.45}Cr_{0.1}Ni_{0.45}O_4$ sample are shown in Fig. 7. The inverse magnetic susceptibility measured at $H = 10$ kOe is shown in Fig. 8 together with that of the disordered $LiMn_{1.5}Ni_{0.5}O_4$ ($Fd\bar{3}m$) phase. The magnetization curves are very similar to those for the same disordered ($Fd\bar{3}m$) phase $LiMn_{1.5}Ni_{0.5}O_4$ shown in Fig. 9. The two samples undergo a magnetic transition at a temperature T_C that is lower by about 12 K in $Li[Ni_{1.45}Cr_{0.1}Ni_{0.45}]O_4$. We argue that this result signals a reduced amount of short-range order of the Ni^{2+} and Mn^{4+} ions.

Electron transfer from the half-filled Ni^{2+} σ-bonding e_g orbital to a half-filled Mn^{4+} π-bonding t_g orbital in a 90° Ni^{2+}-O-Mn^{4+} interaction via a common pσπ orbital is restricted by the Pauli exclusion principle to give an antiferromagnetic Ni^{2+}-Mn^{4+} interaction [16]. Ordering of the Ni^{2+} and Mn^{4+} ions in the $P4_332$ $Li[Ni_{0.5}Mn_{1.5}]O_4$ long-range-ordered phase has been shown to give a ferrimagnetic phase at T_C with antiferromagnetic coupling between the Ni^{2+} and Mn^{4+} sublattices [17]. Frustrated magnetic interactions in a completely disordered phase would give a much lower magnetic ordering temperature than in the ordered phase. Therefore, the existence of long-range magnetic order below a T_C similar to that of the ordered $P4_332$ phase is a signature of a strong correlation function $C_{ij} = \langle P(\mathrm{Mn})_i P(\mathrm{Ni})_j \rangle$ with $P(\mathrm{Mn})_i$ $P(\mathrm{Ni})_j$ the probability that if site i is occupied by Mn, site j is occupied by Ni and C_{ij} is large if i and j are nearest 16d-sites. The fact that the peaks of the XRD spectra reported above are well-described in the framework of the disordered ($Fd\bar{3}m$) phase means that the correlation length C_{ij} is smaller than the length scale probed by XRD,

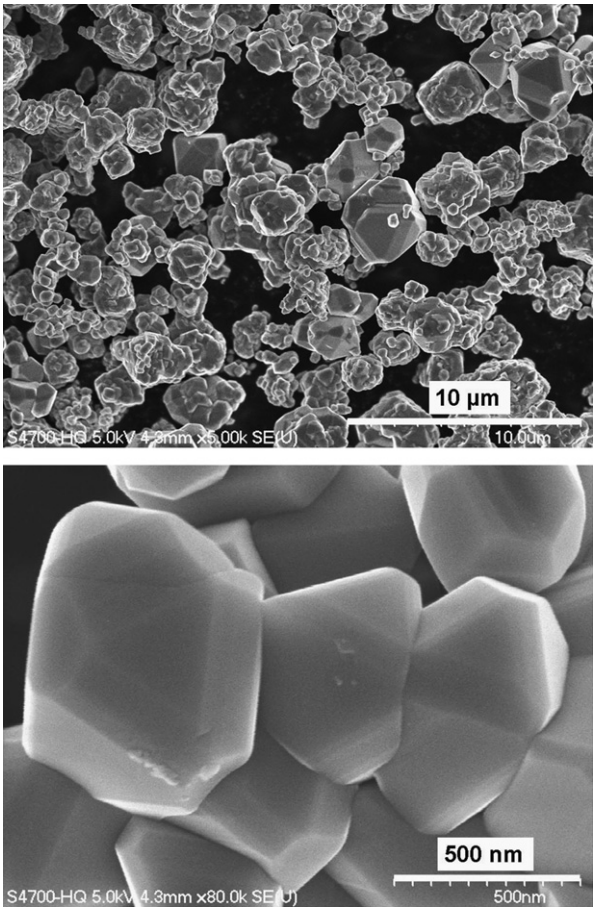

Fig. 6. SEM images of the $LiMn_{1.45}Cr_{0.1}Ni_{0.45}O_4$ samples after post annealing at 600 °C.

typically a few nm (only an analysis of the diffusive X-ray scattering would give access to the correlation function at shorter length scale). The FTIR in the previous section, which is a probe at the molecular scale, already gave evidence of short-range ordering at

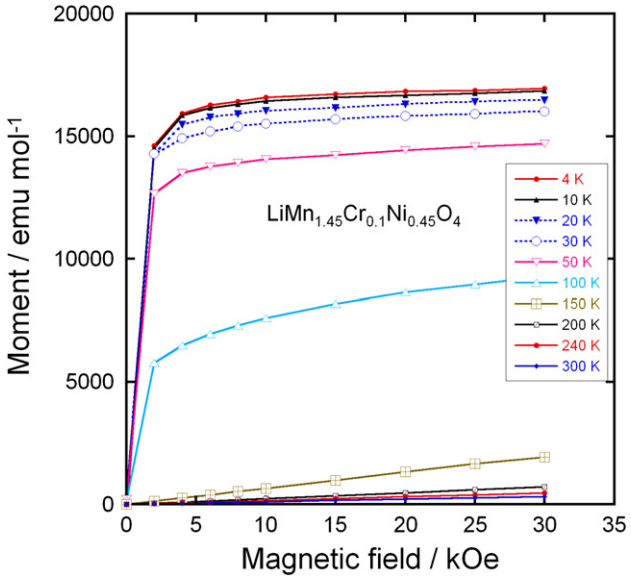

Fig. 7. Magnetization curve of the $LiMn_{1.45}Cr_{0.1}Ni_{0.45}O_4$ samples after post annealing at 600 °C.

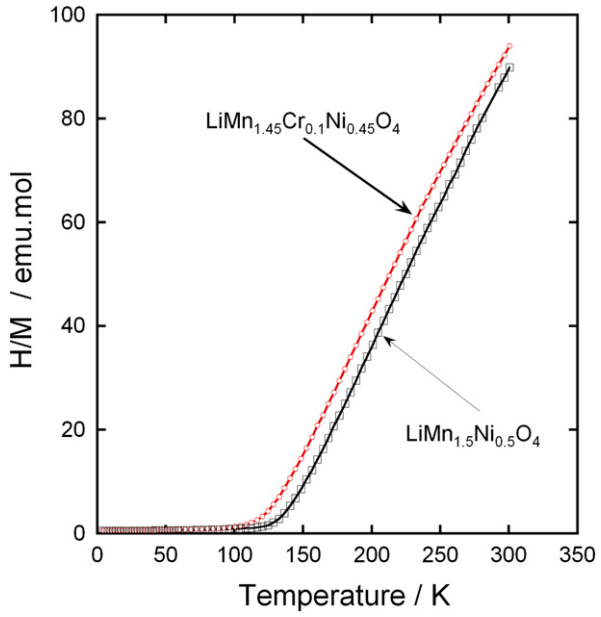

Fig. 8. Inverse magnetic susceptibility defined as H/M with M the magnetization measured at 10 kOe for the $LiMn_{1.45}Cr_{0.1}Ni_{0.45}O_4$ samples after post annealing at 600 °C and the $LiMn_{1.5}Ni_{0.5}O_4$ crystallized in the same $Fd\bar{3}m$ space group.

this scale. The short-range order is confirmed by the magnetic experiments, which are a probe at the atomic scale and show that the crystal has a large degree of order at the scale of the nearest neighbors.

For long-range order, the saturation magnetization at low temperature results from the difference between the magnetic moment carried by Mn^{4+} and Ni^{2+}. The orbital momentum at Mn^{4+} and Ni^{2+} is quenched by the crystal field, which makes a spin-only atomic magnetic moment a good approximation. The spins of Mn^{4+} and Ni^{2+} are $S = 3/2$ and $S = 1$, respectively, so the magnetic moment at saturation for the ordered $LiMn_{1.5}Ni_{0.5}O_4$ should be $(3 \times 1.5 - 2 \times 0.5) = 3.50\ \mu_B$ per formula unit. The experimental value of the saturation magnetization 3.40 μ_B/formula unit at 4.2 K of the $Fd\bar{3}m$ phase, Fig. 9, is in reasonable agreement with the theoretical value for a fully ordered phase and shows the absence of Ni^{3+} ions that would have raised the magnetic momentum to a larger value, as it has been observed in some cases in LMN, ordered or not. The saturation magnetization in the $LiMn_{1.45}Cr_{0.1}Ni_{0.45}O_4$ sample, according to Fig. 7, is only reduced to 3.2 μ_B per formula unit. This result suggests that the Cr^{3+} are not distributed randomly, but tend to form antiferromagnetically coupled dimers randomly distributed in the lattice. This is actually expected and implicit in the notation $2Cr^{3+} = Ni^{2+} + Mn^{4+}$. Two Cr^{3+} on nearest 16*d* sites form the most favorable configuration to lower the energy for two reasons: first, $2Cr^{3+}$ insures charge neutrality at the molecular scale when substituting for $Ni^{2+}+Mn^{4+}$, thus minimizing the cost in Coulomb energy; second, the ionic radii r satisfy approximately the relation $2r(Cr^{3+}) \approx r(Mn^{4+})+r(Ni^{2+})$, so that this substitution also minimizes the lattice distortion. The concentration of Cr is only 5% of the metal ions, *i.e.* far smaller than the percolation of the 16*d*-site sublattice, which is not dense enough to destroy the long-range ferrimagnetic ordering at finite temperature, but it is responsible for a decrease in the short-range Mn^{4+},

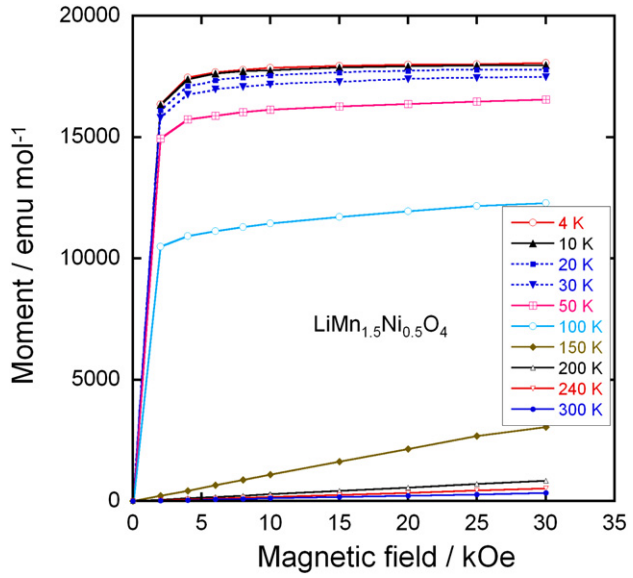

Fig. 9. Magnetization curves of the $LiMn_{1.5}rNi_{0.5}O_4$ sample crystallized in the $Fd\bar{3}m$ space group.

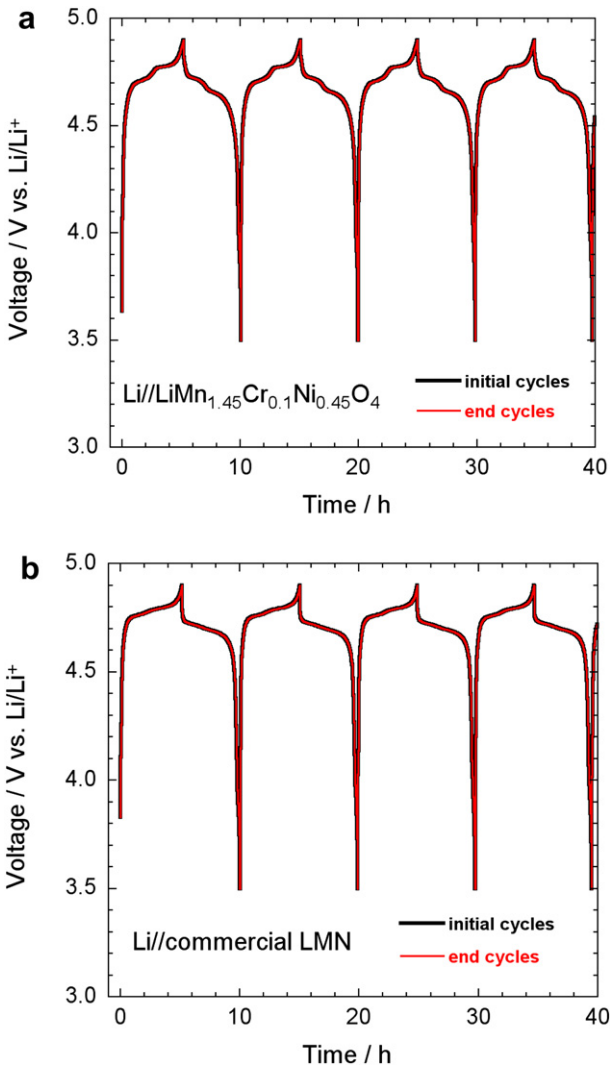

Fig. 10. Voltage profiles of the (a) $LiMn_{1.45}Cr_{0.1}Ni_{0.45}O_4$ and (b) commercial LMN at 0.2C rate. The first five charge/discharge curves are the black lines, while the last five charge/discharge curves are the red lines. (For interpretation of the references to color in this figure legend, the reader is referred to the web version of this article.)

Ni^{2+} order and, therefore of the Néel temperature by 12 K that is observed with respect to $LiMn_{1.5}Ni_{0.5}O_4$. In addition, if we subtract the magnetic moment carried by the Cr^{3+}, 0.3 μ_B per formula, from the Mn and Ni contribution to the magnetic moment at saturation in the antiferrimagnetic phase of $LiMn_{1.45}Cr_{0.1}Ni_{0.45}O_4$, we find $1.45 \times 3 - 0.45 \times 2 - 0.3 = 3.15$ μ_B in agreement with the experimental value 3.2 μ_B.

The electrochemical properties of our $LiMn_{1.45}Cr_{0.1}Ni_{0.45}O_4$ and a commercial sample were investigated. Fig. 10 (black lines) shows the initial four charge/discharge curves at a low rate of 0.2C. A characteristic 4.1 V Mn^{3+}/Mn^{4+} redox couple is always observed in the pristine or metal-doped LMN cathodes as a result of oxygen loss at high-temperature synthesis [11–13,18]. However, no obvious 4.1 V step is detected in our final $LiMn_{1.45}Cr_{0.1}Ni_{0.45}O_4$ spinel (Fig. 10a), confirming that most of the residual Mn^{3+} ions have been re-oxidized to Mn^{4+} after re-annealing at 600 °C in agreement with the analysis of magnetic properties. This is also consistent with the Rietveld refinement result above. In addition, $LiMn_{1.45}Cr_{0.1}Ni_{0.45}O_4$ shows two distinct plateaus at around 4.7 V. In contrast, the commercial sample only exhibits a flat voltage profile at about 4.7 V and no 4.1 V Mn^{3+}/Mn^{4+} plateau. The last five charge/discharge curves after 100 cycles of the $LiMn_{1.45}Cr_{0.1}Ni_{0.45}O_4$ and commercial sample at 0.2C are also reported in Fig. 10 (red lines). In comparison with the initial charge/discharge curves in Fig. 10, similar two voltage plateaus were observed for $LiMn_{1.45}Cr_{0.1}Ni_{0.45}O_4$ and a single voltage plateau for commercial LMN. No obvious change was found after 100 cycles at various C rates, suggesting good reversibility of both samples.

In order to understand the difference in the electrochemical properties of the $LiMn_{1.45}Cr_{0.1}Ni_{0.45}O_4$ and the commercial LMN sample, Fig. 11 compares the dQ/dV *vs.* V graphs, where $Q = \int Idt$ from t=0 at 3.5 V to t at V−3.5. Removal of Li from the tetrahedral sites of the spinel LMN framework initially probes the oxidation reaction of $Ni^{2+} \rightarrow Ni^{3+}$ just below 4.7 V (typically ~4.69 V) for the disordered $Fd\bar{3}m$ and above 4.7 V (typically ~4.72 V) for the ordered $P4_332$ spinels [19]. Ordering of the Ni and Mn raises by ~0.02 eV the $V(x)$ profile of LMN. From Fig. 11a, two anodic peaks at 4.663 and 4.731 V plus two cathodic peaks at 4.638 and 4.704 V were observed for the $LiMn_{1.45}Cr_{0.1}Ni_{0.45}O_4$, which is in agreement with two voltage plateaus for disordered LMN [3,19]. Kim et *al.* suggested that as the crystallographic structure changed from $Fd\bar{3}m$ to $P4_332$, the voltage gaps between the two plateaus became narrower at around 4.75 V and resulted in a flatter voltage profile [8].

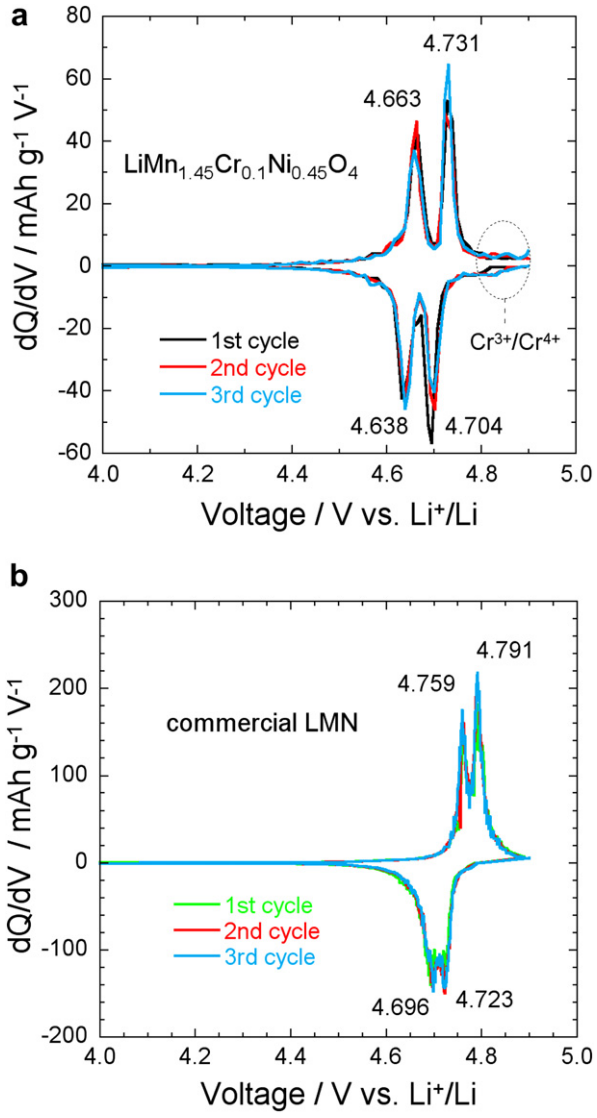

Fig. 11. Differential capacity curves, dQ/dV vs. V, of the (a) $LiMn_{1.45}Cr_{0.1}Ni_{0.45}O_4$ and (b) commercial LMN. The values at the peaks are given in volt.

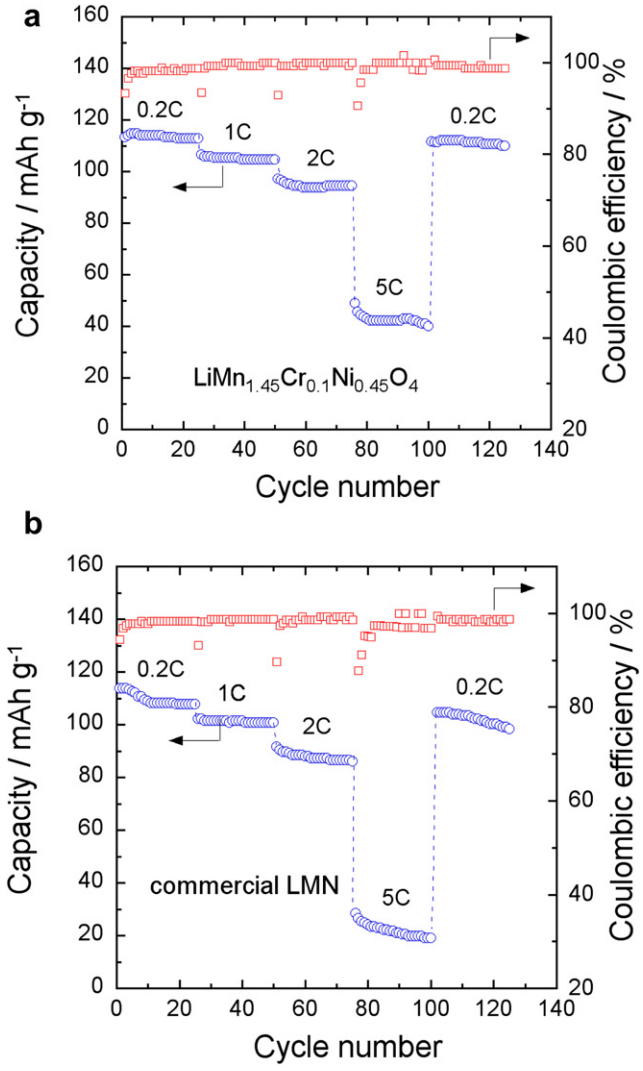

Fig. 12. Cycling performance and columbic efficiency of the (a) $LiMn_{1.45}Cr_{0.1}Ni_{0.45}O_4$ and (b) commercial LMN at various C rates.

Table 1
Capacity loss after 25 cycles for $LiMn_{1.45}Cr_{0.1}Ni_{0.45}O_4$ and commercial LMN at each C rate.

	Initial 0.2C	1C	2C	5C	Last 0.2C
$LiMn_{1.45}Cr_{0.1}Ni_{0.45}O_4$	1.7%	1.9%	2.8%	16.3%	1.2%
Commercial LMN	5.4%	1.3%	6.1%	32.4%	5.8%

This separation is known to decrease from about 60 mV to around 20 mV, depending on the degree of ordering [8,15,19]. The average potential difference, ΔV, between these two peaks is ca. 60 mV for the Cr-doped LMN material and 30 mV for the commercial sample. Therefore these results corroborate the major improvement of the structural order induced by the Cr-doping. The smaller ΔV in commercial LMN compared to that $LiMn_{1.45}Cr_{0.1}Ni_{0.45}O_4$ suggests faster lithium insertion/extraction kinetics in the former [20]. Additionally, small redox peaks were observed in the $LiMn_{1.45}Cr_{0.1}Ni_{0.45}O_4$ at about 4.85 V, showing the redox reaction between Cr^{3+} and Cr^{4+} and confirming the electrochemical activity of Cr in the Cr-substituted LMN.

Fig. 12 shows the cyclability and coulombic efficiency of the $LiMn_{1.45}Cr_{0.1}Ni_{0.45}O_4$ and commercial LMN at different C rates. The capacity loss at each rate is compared in Table 1. It is necessary to note that only 6% of conductive carbon was used to make the cathode electrode in this work. From Fig. 12 and Table 1, the $LiMn_{1.45}Cr_{0.1}Ni_{0.45}O_4$ exhibits better rate capability and capacity retention than commercial LMN. For instance, the $LiMn_{1.45}Cr_{0.1}Ni_{0.45}O_4$ delivered a reversible capacity of ~115, 104, 95 and 40 mAh g^{-1} at 0.2C, 1C, 2C and 5C, respectively; the commercial LMN offered a lower reversible capacity of ~110, 98, 85 and 20 mAh g^{-1} at the same C rates. When returned to 0.2 C from 5 C after 100 cycles, about 99% of reversible capacity was retained for $LiMn_{1.45}Cr_{0.1}Ni_{0.45}O_4$ *vs.* 94% for commercial LMN.

The rate capability of cathodes is determined by the lithium-ion insertion/extraction kinetics. Insertion/extraction of lithium ions into/from a cathode involves (1) lithium-ion diffusion through any solid state interphase (SEI) layer, (2) the electron-transfer reaction, and (3) lithium-ion diffusion in the bulk of the materials [18]. Electrochemical impedance spectroscopy (EIS) studies were performed to understand better the electrochemical performances of the $LiMn_{1.45}Cr_{0.1}Ni_{0.45}O_4$ and commercial LMN. Fig. 13 compares the EIS spectra of the two samples at open-circuit voltage. The

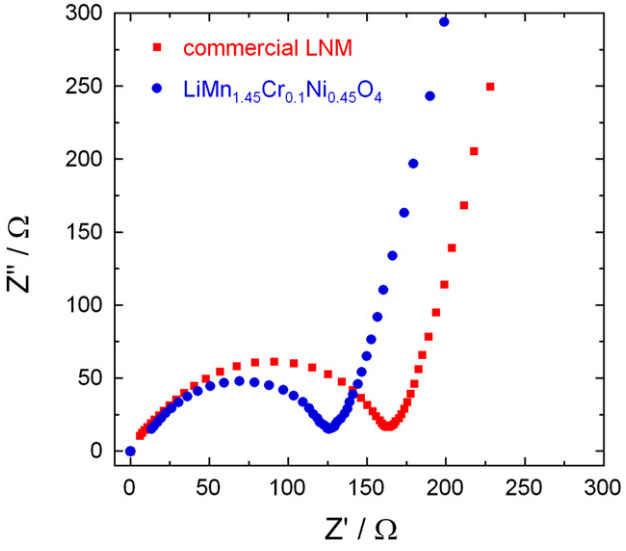

Fig. 13. EIS spectra of the $LiMn_{1.45}Cr_{0.1}Ni_{0.45}O_4$ and commercial LMN at open-circuit voltage.

semicircle in the high-frequency region records the surface resistance R_s, which represents the resistance for lithium-ion diffusion in the surface layer, including SEI layer and/or coating layer, and its value can be determined from the diameter of the semicircle [21]. From Fig. 13, about 125 Ω of R_s was obtained for the $LiMn_{1.45}Cr_{0.1}Ni_{0.45}O_4$, while ~160 Ω of R_s was observed for the commercial LMN. The smaller R_s of $LiMn_{1.45}Cr_{0.1}Ni_{0.45}O_4$ compared to that of commercial LMN suggests faster lithium insertion/extraction kinetics across the electrode/electrolyte interface. Moreover, as previously indicated [12], a little Cr-substitution suppresses the formation of the SEI layer at the surface so as to improve the cathode rate capability. Meanwhile, it is the oxidized surface Ni that reacts with the electrolyte to form SEI layers that impede Li^+-ion diffusion across the electrode/electrolyte interface. In the Cr-substituted spinel, Ni tends to be segregated from the surface to the bulk, which may suppress the electrolyte decomposition and thereby improves the capacity retention.

4. Conclusion

In this work, $LiMn_{1.45}Cr_{0.1}Ni_{0.45}O_4$ spinel was prepared by a co-precipitation method assisted by a post-annealing at 600 °C. Structural analyses suggest that a post annealing process at lower temperature is an effective way to tune the oxygen deficiency while keeping the spinel in the disordered structure. Compared with the commercial LMN, the $LiMn_{1.45}Cr_{0.1}Ni_{0.45}O_4$ gave a better rate capability along with capacity retention. EIS measurement revealed that the $LiMn_{1.45}Cr_{0.1}Ni_{0.45}O_4$ had a smaller surface resistance, which may due to the segregation of Ni from the surface to the bulk. The study demonstrates that post annealing at low temperature is a viable strategy to modify the oxygen deficiency and thereby eliminate the impurity phase for the LMN synthesis. Meanwhile, the Cr-segregation also represents a low-cost manufacturing approach compared to a post-chemical coating.

Acknowledgments

The authors would like to acknowledge the support from the U.S. Department of Energy under the BATT program (with Lawrence Berkeley National Laboratory).

References

[1] S. Sawa, S. Okada, A. Yoshino, J. Power Sources 97-98 (2001) 430.
[2] R. Ruffo, R.A. Huggins, C.M. Mari, M. Piana, W. Weppner, Ionics 11 (2005) 213.
[3] J.-H. Kim, S.-T. Myung, C.S. Yoon, S.G. Kang, Y.-K. Sun, Chem. Mater. 16 (2004) 906.
[4] K. Takahashi, M. Saitoh, M. Sano, M. Fujita, K. Kifune, J. Electrochem. Soc. 151 (2004) A173.
[5] M. Kunduraci, J.F. Al-Sharab, G.G. Amatucci, Chem. Mater. 18 (2006) 3585.
[6] N. Amdouni, K. Zaghib, F. Gendron, A. Mauger, C.M. Julien, Ionics 12 (2006) 117.
[7] T. Minami, M. Tatsumisago, M. Wakihara, C. Iwakura, S. Kohjiya, I. Tanaka (Eds.), Solid State Ionics for Batteries, Springer-Verlag, Tokyo, 2005, p. 101.
[8] J.-H. Kim, C.S. Yoon, S.-T. Myung, J. Prakash, Y.-K. Sun, Electrochem. Solid-State Lett. 7 (2004) A216.
[9] M. Kunduraci, G.G. Amatucci, J. Electrochem. Soc. 153 (2006) A1345.
[10] T.A. Arunkumar, A. Manthiram, Electrochim. Acta 50 (2005) 5568.
[11] G.B. Zhong, Y.Y. Wang, Y.Q. Yu, C.H. Chen, J. Power Sources 205 (2012) 385.
[12] D. Liu, Y. Lu, J.B. Goodenough, J. Electrochem. Soc. 157 (2010) A1269.
[13] D.W. Shin, A. Manthiram, Electrochem. Commun. 13 (2011) 1213.
[14] D. Liu, J. Han, J.B. Goodenough, J. Power Sources 195 (2010) 2918.
[15] X. Ma, B. Kang, G. Ceder, J. Electrochem. Soc. 157 (2010) A925.
[16] J.B. Goodenough, Magnetism and the Chemical Bond, Wiley, New York, 1963.
[17] N. Amdouni, K. Zaghib, F. Gendron, A. Mauger, C.M. Julien, J. Mag. Mater. 309 (2007) 100.
[18] J. Liu, A. Manthiram, J. Phys. Chem. C 113 (2009) 15073.
[19] M. Kunduraci, G.G. Amatucci, J. Power Sources 165 (2007) 359.
[20] F.G.B. Ooms, E.M. Kelder, J. Schoonman, M. Wagemaker, F.M. Mulder, Solid State Ionics 152 (2002) 143.
[21] J. Liu, A. Manthiram, J. Electrochem. Soc. 156 (2009) A833.